# Splitting of Material Cells and Averaging Properties to Improve Accuracy of the FDTD Method at Interfaces

R. S. Schechter, M. Kragalott, M .S. Kluskens, and W. P. Pala

Authors are in Code 5310 of the Radar Division at the Naval Research Laboratory, Washington DC 20375
(schechter@cem.nrl.navy.mil)

**Abstract - In this paper we present a simple modification to the traditional Finite Difference Time Domain (FDTD) method for treating material cells. The Yee cell is split into 8 smaller material subcells so that each E and H field point is considered to be located at the crosspoint of 8 cells with differing material properties. Thus there is no longer an overlap of the material cells associated with the components of the E and H fields. The 8 material properties are averaged at each crosspoint. Since the averaging is done outside the time marching loop there is little increase in the total computational time. Numerical results are shown for a sinusoidal plane wave scattering from a dielectric sphere. These results are compared with the exact Mie solution and the traditional material cell method along different cuts through the sphere. The splitting and averaging is shown to give improved amplitude accuracy in the vicinity of the sphere. Improvement is also observed at planar interfaces angled with respect to the grid. An additional benefit of this subcell formulation is that objects may be modeled with twice the geometrical resolution without increasing the size of the staggered grid.**

**Index Terms- FDTD, Subcell, Split cell, Effective Dielectric Constant**

## I. INTRODUCTION

The finite-difference time domain (FDTD) technique is a widely used method for computing electromagnetic scattering. The formulation is based on the ideas put forth in [1] and involve computing the electric and magnetic (E and H) fields on a staggered grid. There are some shortcomings with the Yee method when applied to interfaces between materials. First, the material cells associated with the field components (staggered in space) are centered around each field point and thus overlap in space. Second, the discontinuity in permittivity at interfaces between different media causes accuracy problems. Third, is the error caused by approximating a curved boundary by a staircased one.

Various methods have been proposed to improve the accuracy of the basic FDTD method at interfaces, mainly by reducing the staircasing errors caused by angled or curved boundaries. For example, one method uses a volume weighted average of $\varepsilon$ on each side of a material interface [2]. An effective dielectric constant is computed as follows:

$$\varepsilon_{eff} = (V_1\varepsilon_1 + V_2\varepsilon_2)/V_{cell}\,, \qquad (1)$$

where $V_1$ is the volume on one side of the interface and $V_2$ is the volume on the other side of the interface. This method requires a special treatment of each material interface. Specifically the method requires identifying which cells are intersected by the boundary and where the boundary intersects these cells. Dey and Mittra reported that the results using this approach are significantly more accurate than using a staircase to approximate the surface of a dielectric structure. Another approach uses effective dielectric constants together with the contour-path integral FDTD (CFDTD) method [3]. Recently a new technique was developed that utilizes the electric field components along the edges of the cell [4]. Rather than using the volume of the dielectric occupying a cell it instead uses the length of the dielectric intersecting the cell edges.

Still another method uses dielectric subgrid resolution (DSR) [5]. This can be described as partitioning a standard cell into 8 subcells, each homogeneously filled. The 8 cells can have different material properties. Generalized constitutive parameters are obtained by treating each cell as an equivalent lumped circuit. It is shown by numerical example that on coarser grids the simpler averaging method gives more accuracy than the lumped circuit approach across interfaces. The DSR method also requires greater memory since there are effective dielectric constants for 3 directions.

The practical advantage to the approach presented in this paper is that no special preprocessing operations are required to compute the intersections of cells with interface boundaries. The comparisons in this paper are on the basis of field amplitudes as opposed to resonance frequencies used in the cited articles.

## II. SIMPLE SUBCELL MODEL

The method presented here uses the standard staggered grid scheme but now sub-divides or splits the existing cell into 8 smaller cells as shown in Fig. 1. Each field point may now be viewed as a crosspoint surrounded by 8 subcells with differing parameters as

opposed to being at the center of a material cell. The material cells no longer overlap in space for the staggered field points. A sphere, for example, cutting through the standard Yee cell still is approximated with a staircase but with twice the number of cells. Unlike some previous approaches there are no special calculations related to the specific geometry modeled.

Applying Ampere's Law around a contour $C_1$ one obtains:

$$\frac{\partial}{\partial t}\int_{S_1}\vec{D}\cdot d\hat{S}_1 = \oint_{C_1}\vec{H}\cdot d\hat{l}_1 . \qquad (2)$$

From Fig. 1, assuming that $D_z$ is constant over a surface patch $S_1$ (center x-y plane in Fig. 1) and is equal to the value at the center of the patch, the surface integral becomes:

$$\int_{S_1} D_z dS = \varepsilon(i,j,k)E_z\Big|_{i,j,k}\Delta x\Delta y . \qquad (3)$$

Assume also that the value of the $H$ field along each contour leg is constant and equal to the value at the midpoint of the leg. Since the material cell is now split, further assume that at the cell center $(i,j,k)$ or crosspoint of the 8 material cells, that the effective dielectric constant is the average of the 8 surrounding material cells or :

$$\varepsilon(i,j,k) = \bar{\varepsilon}(i,j,k) = 1/8\sum_{n=1}^{8}\varepsilon_n . \qquad (4)$$

Using central-difference approximations for the time derivatives (interleaved in time) the following step-ahead equation results - valid for non-cubical cells.

$$\begin{aligned} E_z^{n+1}\Big|_{i,j,k} = E_z^n\Big|_{i,j,k} + \frac{\Delta t}{\bar{\varepsilon}(i,j,k)}\Bigg[ & \frac{1}{\Delta y}H_x^{n+1/2}\Big|_{i,j-1/2,k} \\ & + \frac{1}{\Delta x}H_y^{n+1/2}\Big|_{i+1/2,j,k} \\ & - \frac{1}{\Delta y}H_x^{n+1/2}\Big|_{i,j+1/2,k} \\ & - \frac{1}{\Delta x}H_y^{n+1/2}\Big|_{i-1/2,j,k}\Bigg] \end{aligned} \qquad (5)$$

Analogous equations can be developed for $E_y$ and $E_x$ .

## III. BENCHMARK PROBLEM - DIELECTRIC SPHERE

The problem considered is a plane wave scattering from a dielectric sphere. The incident wave has the electric field polarized in the z direction and travels in the +y direction as shown in Fig. 2. The dielectric sphere has a radius of 4.5 cm. In this work we consider scattering at two frequencies and two dielectric constants. Case I is at a frequency of 2.5 GHz with $\varepsilon = 4\varepsilon_0$ in the sphere and Case II is at 1.768 GHz with $\varepsilon = 8\varepsilon_0$ in the sphere. In each case the wavelength in the sphere is the same. The Mie series solution for the fields inside and outside the sphere is compared to numerical FDTD results.

### A. Computational Modeling

Numerical results are generated using a 3D FDTD computational code that implements the standard Yee method with and without the subcell averaging. The computational grid is 512 x 256 x 512. At the extremities of the grid Liao second order absorbing boundary conditions (ABC'S) are employed. A sine wave source is fed in at y=5. The incident wave is planar over 1/2 of the grid's width or from x= 128 to x=384, with a Gaussian taper toward the absorbing boundaries This finite-width waveform approximates plane wave conditions in the vicinity of the sphere. The spatial discretization $\Delta x$ is set to $\lambda/20$ (in the dielectric media) for both Cases I and II. The sphere has a radius of $15\,\Delta x$ ;however, with the split cell model, the sphere has a radius of 30 subcells. The FDTD simulation is run in continuous wave (cw) mode, long enough to achieve steady-state conditions over the extent of the grid. The amplitudes of the vector components of the E field are saved along chosen line cuts (along y) though the sphere. The program, which updates large 3D grids, is written with OpenMP directives to run efficiently on an SGI Origin parallel computer.

### B. Analytical Solution

The Mie solution for a plane harmonic wave scattering from a dielectric sphere is well known and may be found in several references [6,7]. This exact solution is a series for the scattered field exterior to the sphere and the transmitted or total field interior to the sphere. The incident field is added to the scattered field to obtain the total field outside the sphere. The resulting vector components, in spherical polar coordinates, are transformed into Cartesian vector components along various cuts though the sphere. This permits a direct comparison with the FDTD solution. Care must be taken to insure that the FDTD cuts correspond exactly in space with the analytical ones.

### C. Results and Comparison

Fig. 3 shows comparisons for Case I between the Mie solution (exact), the 8 subcell or split cell model, and standard cell model for the magnitude of $E_z$ along a

straight line through the sphere. For cuts parallel to the y-axis, $E_z(0,y,0)$ in Fig. 3(a) and $E_z(8,y,0)$ in Fig. 3(b), the standard cell, the split cell and exact results are close and difficult to distinguish. However, the standard cell model exhibits a local amplitude overshoot at the back of the sphere. The subcell model produces more accurate field values at the back of the sphere.

Fig. 4 shows the comparison between the Mie solution, the subcell model, and the standard model for the magnitude of $E_y$. Along the cut $E_y(0,y,1)$ shown in Fig.4(a), the standard cell model gives a large undershoot and spatial phase error near the back of the sphere, where there is a discontinuity in $E_y$. The subcell model does not exhibit this large undershoot or spatial error. The standard cell model also overshoots the exact solution near the front of the sphere. Fig. 4(b) shows the cut $E_y(0,y,8)$. The standard cell and split cell are closer in amplitude away from the center (z=0) plane.

Figs. 5 and 6 show the analogous comparisons for Case II. A rather large overshoot is apparent in Fig. 5(b) near the back of the sphere in the z=8 plane for the standard cell case. Fig. 6(a) best illustrates the standard cell errors and shows large undershoots at both the front and back of the sphere, where there are jump discontinuities in $E_y$. An overshoot at the back of the sphere for the standard cell method is also apparent in Fig. 6(b). The split cell model agrees better with the exact at both the front and back of the sphere.

To compare the split cell and averaging method with the similar dielectric subgrid resolution (DSR) method [5]. Case II was computed using a grid spacing of 1/10 of a wavelength in the sphere. This coarse grid accentuates any differences between the methods. The $E_y$ component across the interface best illustrates these differences. Fig. 7(a) shows that the DSR method tends to underestimate the jump discontinuities as compared to the simpler averaging method. However, at 1/20 of a wavelength in the sphere, the DSR and simple averaging curves are both converging to the Mie result, as shown in Fig.7(b).

## IV. PLANAR INTERFACES

The performance of the split cell FDTD method is further demonstrated by computing the reflection and transmission of a plane wave Gaussian pulse polarized in the z direction from a planar interface. The grids are chosen to be 128×64×128. An interface tilted at 14° is simply a wedge angled from (0,64,z) to (128,128,z). The grid spacing is based on the 2/3 down power point for the pulse. At this frequency the grid spacing is chosen to be 1/10 of a wavelength in the dielectric. At smaller grid spacings the differences between the split cell and standard cell become minimal for a single pulse. For 1/10 of a wavelength grid spacing in the dielectric a second-order accurate FDTD formulation is used. The same cases are repeated with a coarser grid spacing of 1/7.5 of a wavelength but using a fourth-order (second-order in time and fourth-order in space or 2,4 scheme) FDTD formulation.

The peak amplitudes of the transmitted pulse and reflected pulse are compared with the exact amplitudes. In order to capture the reflected amplitude the incident pulse is subtracted out on the reflecting side of the interface. The results are summarized in Tables I-IV. The percent errors are shown in parentheses. The data show that the split cell formulation is consistently more accurate for interfaces angled at 14°. The cell splitting and averaging is particularly useful on coarse grids where staircasing errors may be more of a concern. The split cell and standard cell give the same transmitted and reflected amplitudes for 0° (normal incidence) thus illustrating that the averaging only has an effect for interfaces at angles.

## V. CONCLUSIONS

The split cell and averaging method is shown to give improved accuracy across angled interfaces and along curved interfaces, such as a sphere. The method is especially useful where coarser grids are required. The technique is very simple, only requiring that the material cells have twice the resolution of the field cells. Since the averaging of the dielectric constants is done prior to the time stepping of the fields there is little added computational cost.

## ACKNOWLEDGEMENTS

The authors wish to thank the Department of Defense High Performance Computing Program for providing the computing resources. This work was funded by the 6.1 basic research program at the Naval Research Laboratory.

## REFERENCES

[1] K. S. Yee, "Numerical solution of initial boundary value problems involving Maxwell's equations in isotropic media," *IEEE Trans. Antennas and Propagation*, Vol. 14, pp. 302-307, May 1966.

[2] S. Dey and R. Mittra, "A conformal finite-difference time-domain technique for modeling cylindrical dielectric resonators," *IEEE Trans. Microwave Theory and Techniques*, Vol. 47, pp. 1737-1739, Sept. 1999.

[3] N. Kaneda, B. Houshmand, and T. Itoh, "FDTD Analysis of Dielectric Resonators with Curved Surfaces," *IEEE Trans. Microwave Theory and Techniques*, Vol. 45, pp.1645-1649, Sept. 1997.

[4] W. Yu and R. Mittra, "A Conformal Finite Difference Time Domain Technique for Modeling Curved Dielectric Surfaces," *IEEE Microwave and Wireless Components Letters*, Vol. 11, pp.25-27, Jan. 2001.

[5] G. Marrocco, M. Sabbadini, and F. Bardati, "FDTD Improvement by Dielectric Subgrid Resolution, "*IEEE Trans. Microwave Theory and Techniques*, Vol. 46, pp. 2166-2169, Dec. 1998.
[6] J. A. Stratton, *Electromagnetic Theory*, New York and London: McGraw-Hill, 1941.
[7] M. N. O. Sadiku, *Numerical Techniques in Electromagnetics*, Boca Raton, London, New York, Washington D.C.:CRC Press 2001.

Richard Schechter is a physicist in the Radar Division at Naval Research Laboratory in Washington DC. His current interests are the finite-difference time domain (FDTD) method, parallel computing, and computational electromagnetics. He also has conducted reasearch and published articles on simulating ultrasonic wave propagation on parallel computers. He obtained his B.S. in Physics from the University of Maryland in 1974 and took further graduate studies in physics and applied mathematics 1974-1980 at American University and Catholic University, both in Washington DC.

Mark Kragalott received the B.A. degree in physics and economics at Kenyon College in 1983, and M.S. and Ph.D. degrees in electrical engineering from The Ohio State University, in 1988 and 1993, respectively. As a Graduate Research Associate at the ElectroScience Laboratory at The Ohio State University, he conducted research on method of moments and extremely low frequency shielding. Since 1994 he has been with the Electromagnetics Section in the Analysis Branch of the Radar Division at the Naval Research Laboratory, Washington, D.C, where he has conducted research in topics ranging from computational electromagnetics to ultrawideband radiation and scattering.

Michael S. Kluskens received B.S. and M.S. degrees in electrical engineering from Michigan Technological University, Houghton, MI, in 1984 and 1985, respectively, and the Ph.D degree from The Ohio State University, Columbus, OH, in 1991. From 1986 to 1991, he was a Graduate Research Associate at the Electroscience Laboratory, Department of Electrical Engineering, the Ohio State University, where he conducted research on the method of moments and chiral media. He has been with the Radar Division of the Naval Research Laboratory, Washington D.C. since 1991 and is currently with the Electromagnetics Section of the Analysis Branch of the Radar Division. His primary research is in computational elecltromagnetics with emphasis on the method of moments, finite-difference time domain, and scattering from large complex structures.

William P. Pala received the B.S., M.S. and Ph.D degrees in physics from The American University, Washington, DC, in 1969, 1971, and 1976, respectively. He was a Graduate Research Associate from 1974 to 1977 at the Naval Research Laboratory. He joined the staff of the Naval Research Laboratory, Washington , DC, in 1978 where he is currently the Branch Chief of the Radar Analysis Branch. He has conducted systems research on orbital and naval radar designs. He has been conducting basic and applied research in radar cross-section determination for targets of naval interest for almost two decades. His current research interests are in computational electromagnetics, antennas, ocean scattering, automatic target recognition, and radar signature measurements. Dr. Pala is a member of the IEEE Antennas and Propagation Society and Sigma Phi Sigma physics honor society.

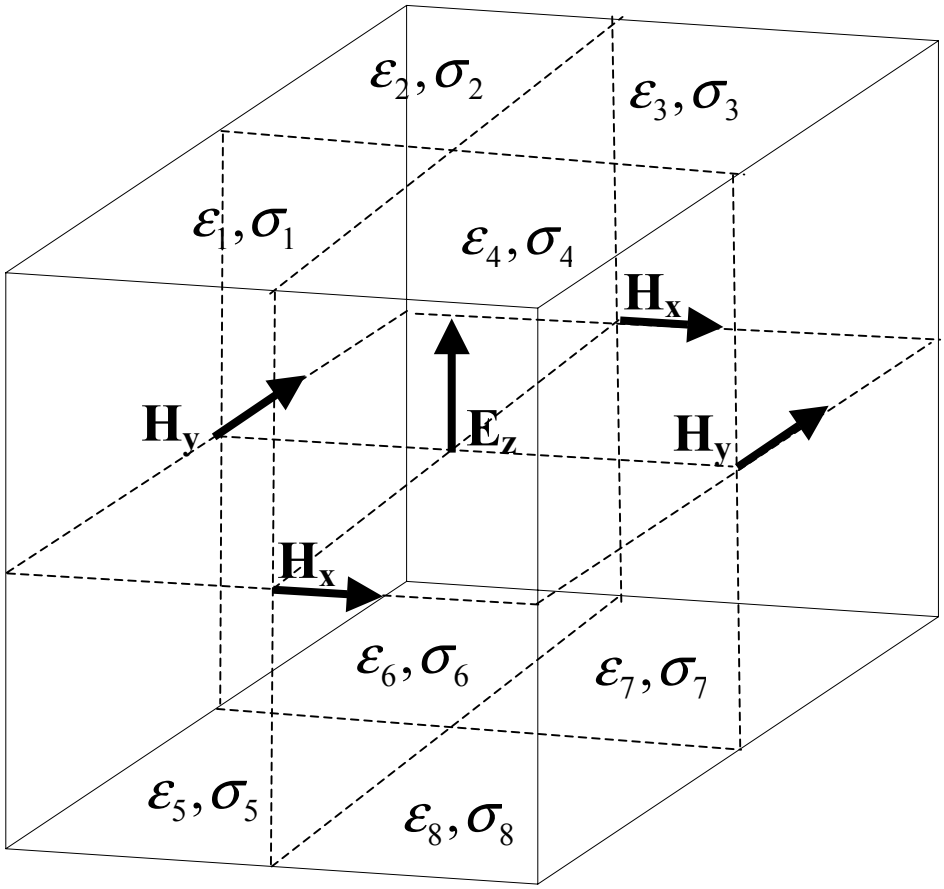


Fig. 1 Diagram of Yee cell with 8 subcells along with the position of the **E** and **H** vector components.

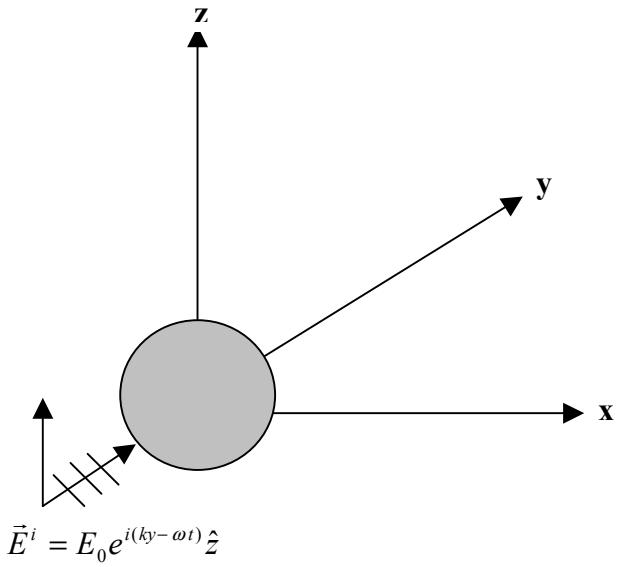


Fig. 2 Diagram of incident wave, dielectric sphere, and coordinate system.

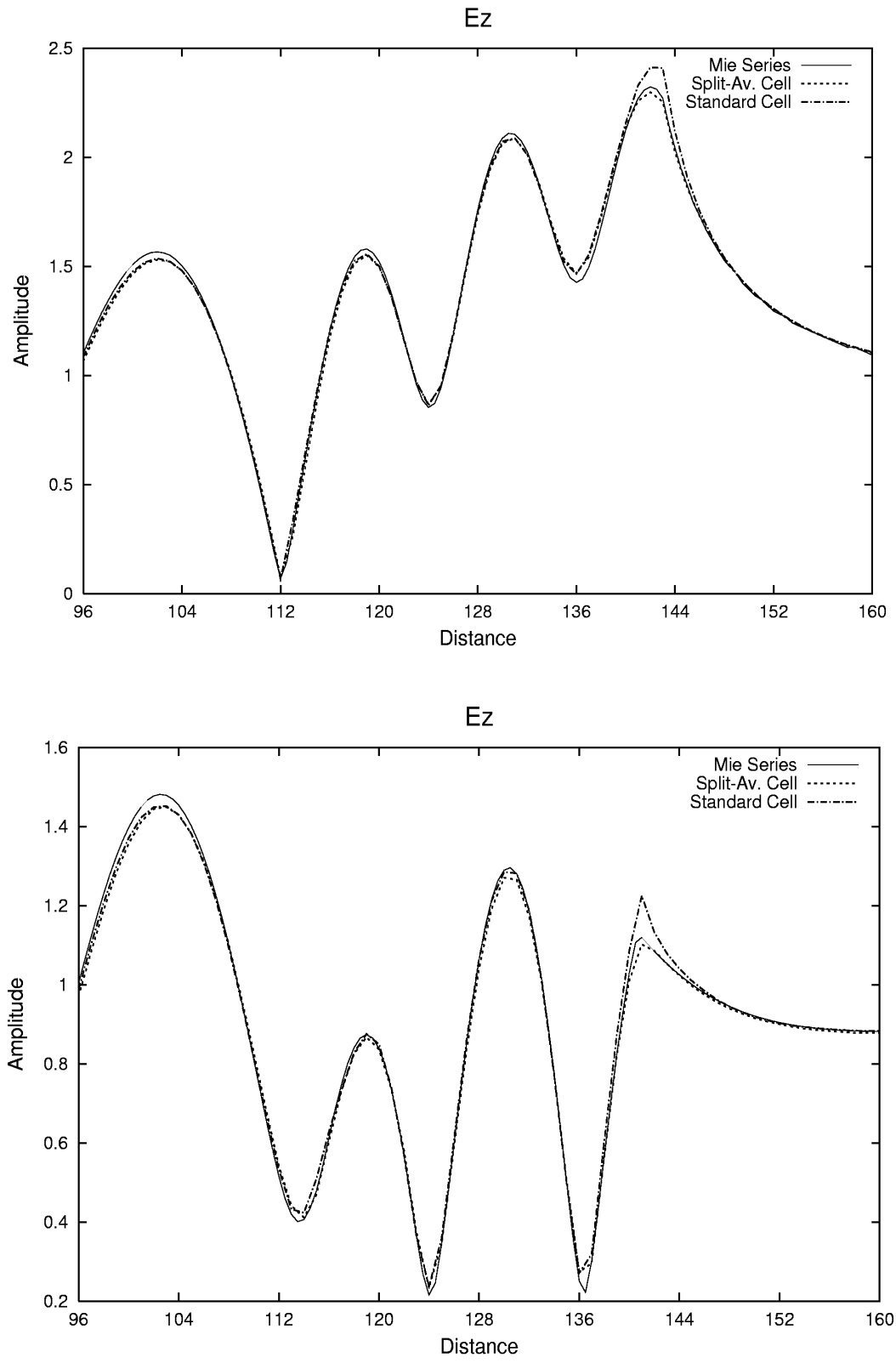


Figure 3a and 3b - Magnitude of $E_z$ parallel to y-axis through (x=0, z=0) and (x=8,z=0). Solid line is exact Mie solution, long dash is standard cell and short dash is split-cell. The sphere is located between y=113 and y=143. Case I, f=2.5 GHz and ε=4.

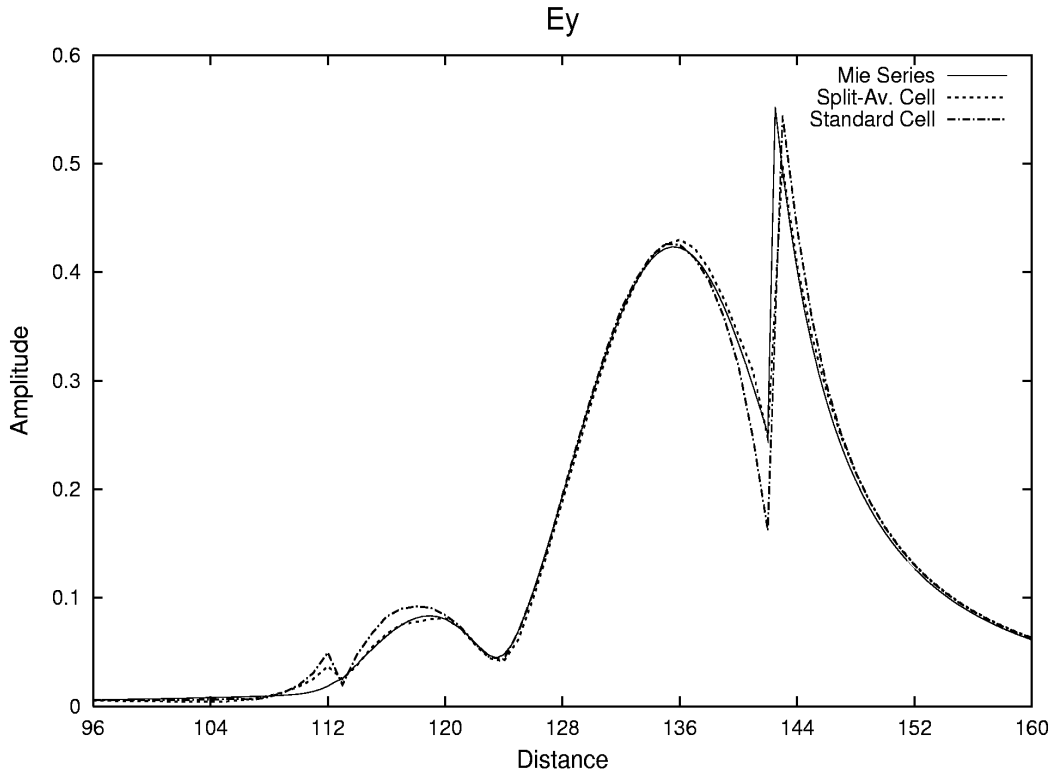


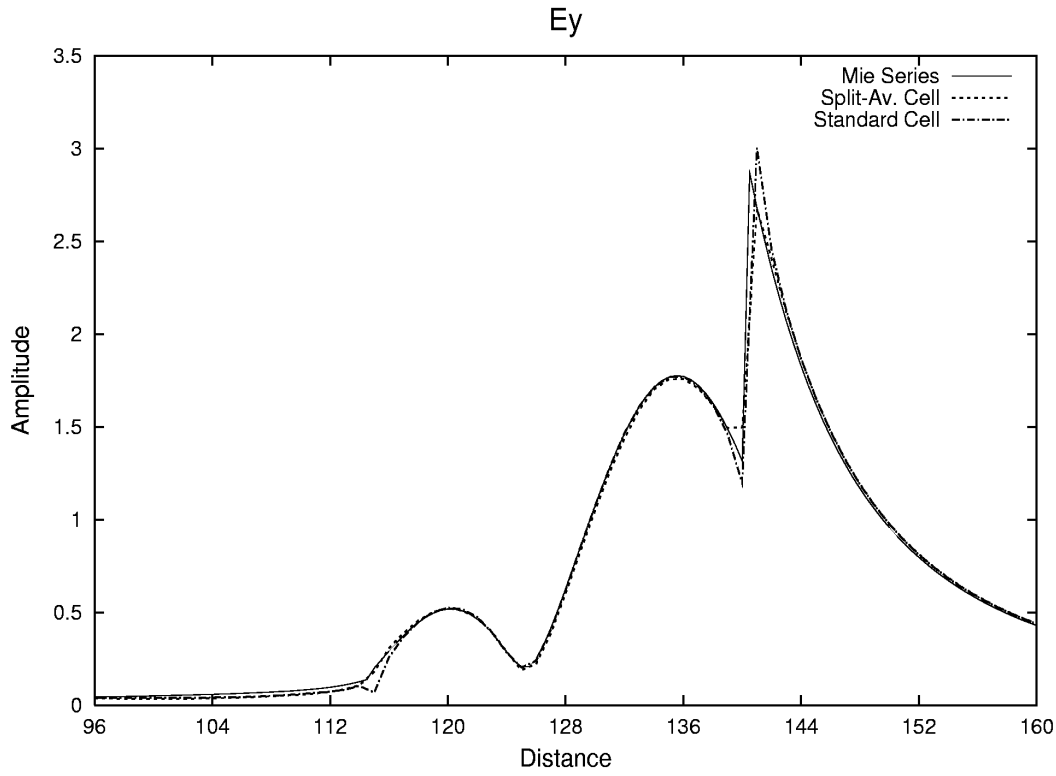


Figure 4a and 4b - Magnitude of $E_y$ parallel to y-axis through (x=0,z=1) and (x=0,z=8). Case I, f=2.5GHz and ε=4.

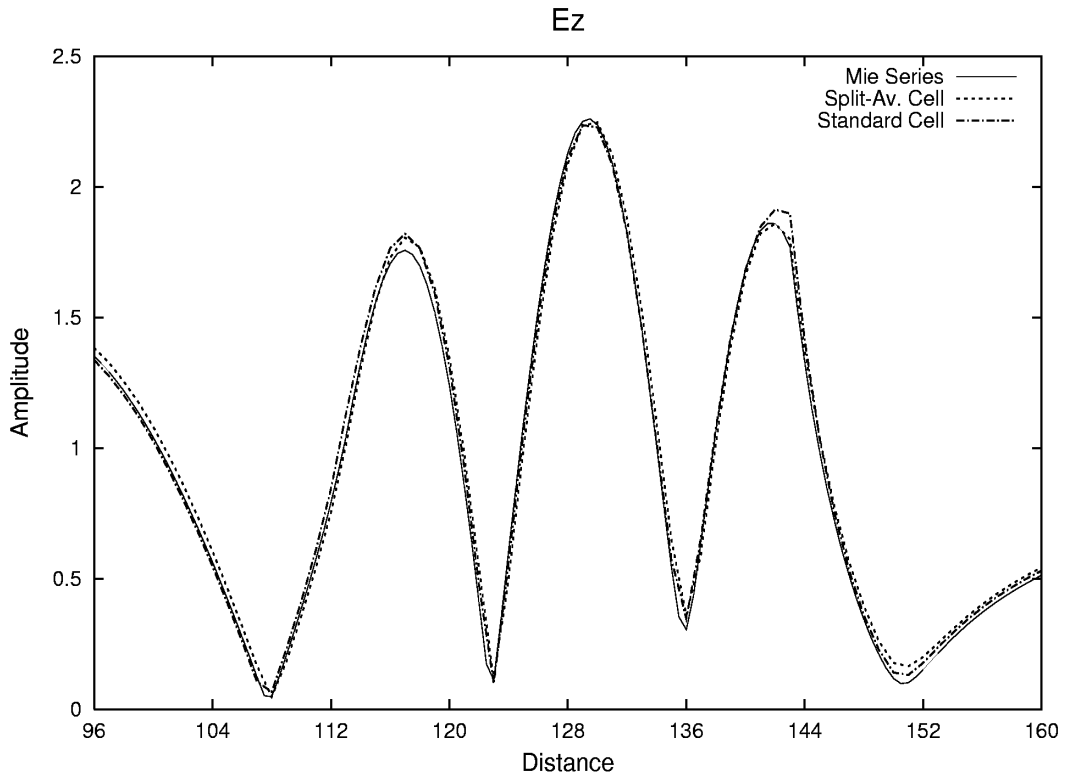


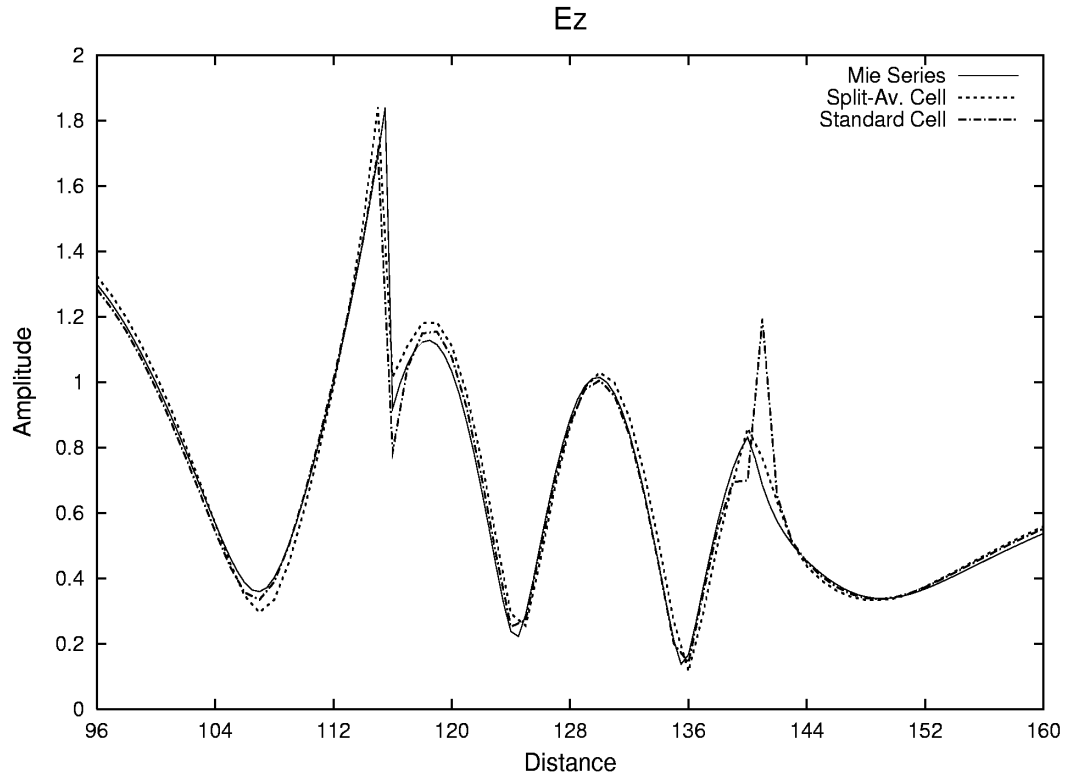


Figures 5a and 5b - Magnitude of $E_z$ parallel to y-axis and through (x=0,z=0) and (x=0, z=8). Sphere is located between y=113 and y=143. Case II, f=1.767 GHz and ε=8.

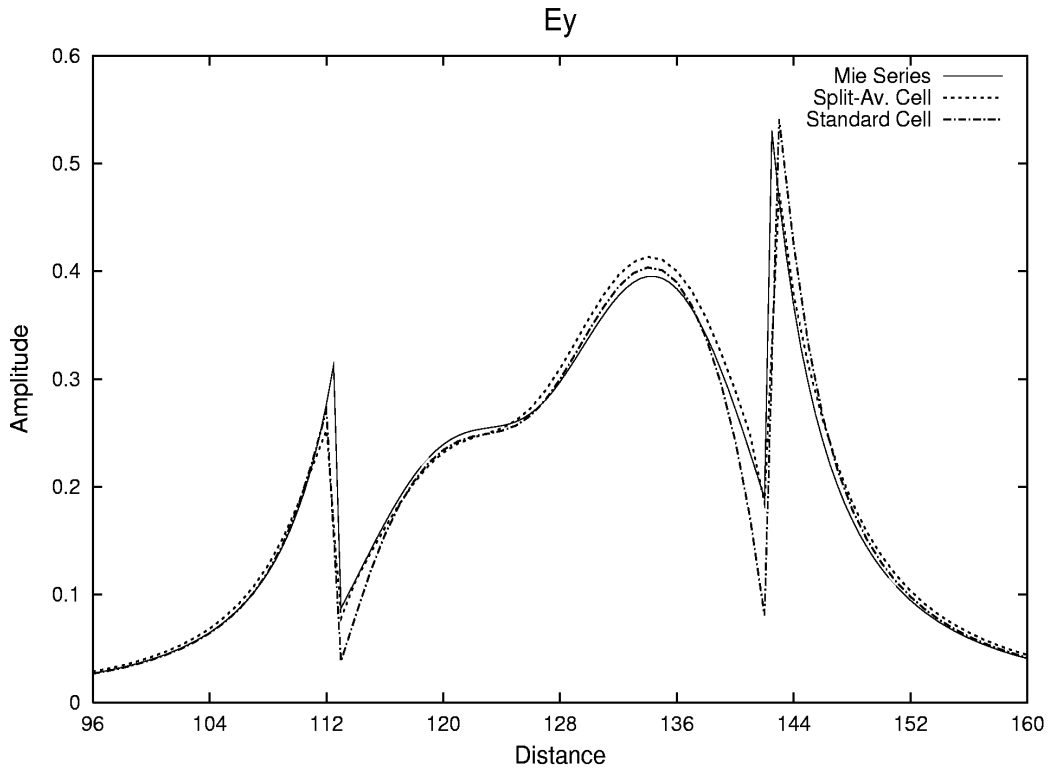


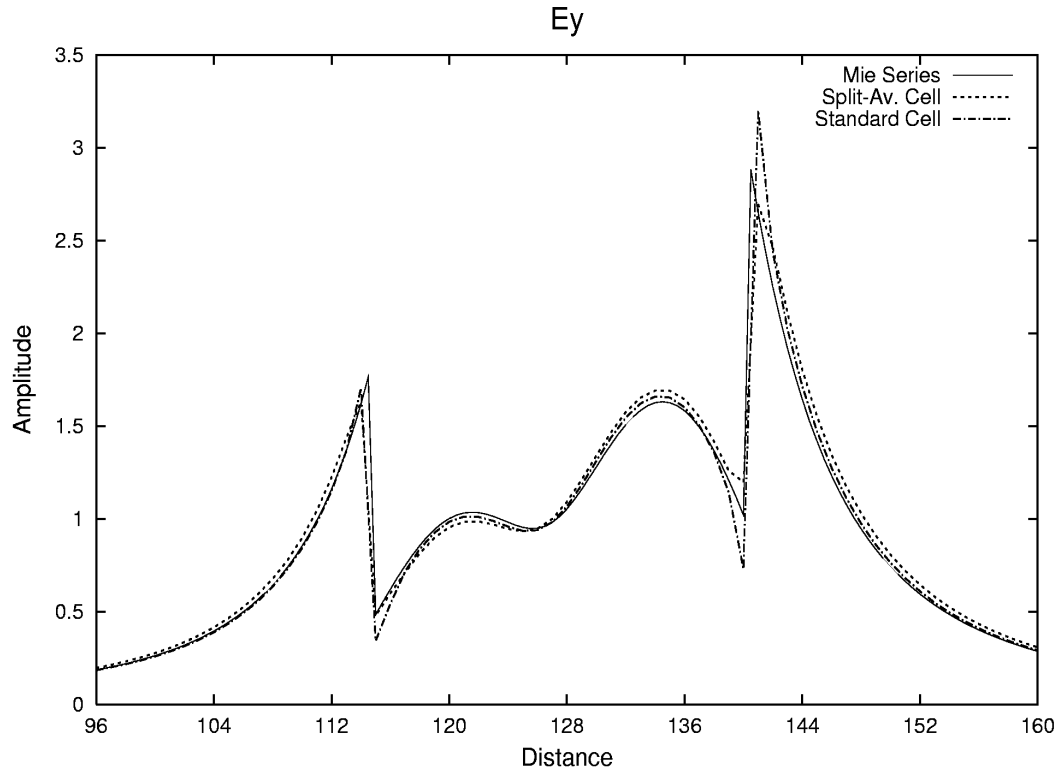


Figures 6a and 6b - Magnitude of $E_y$ parallel to y-axis through (x=0,z=0) and (x=0,z=8). Sphere is located between y=113 and y=143. Case II, f=1.767 GHz and ε=8.

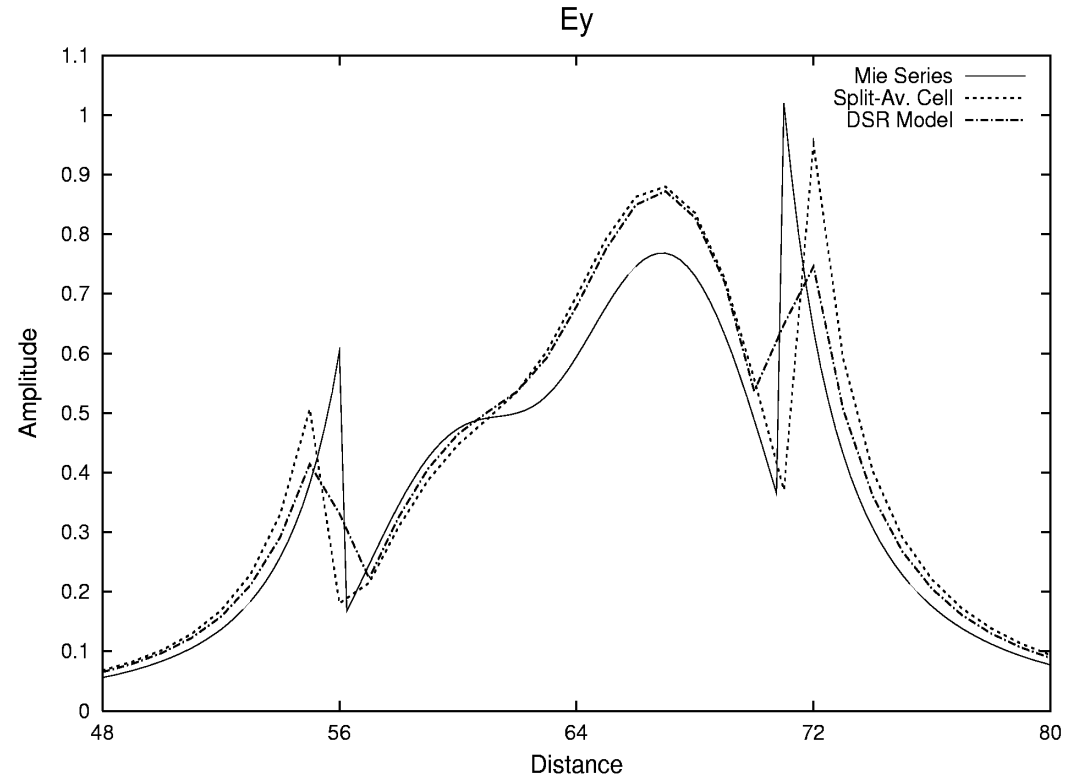


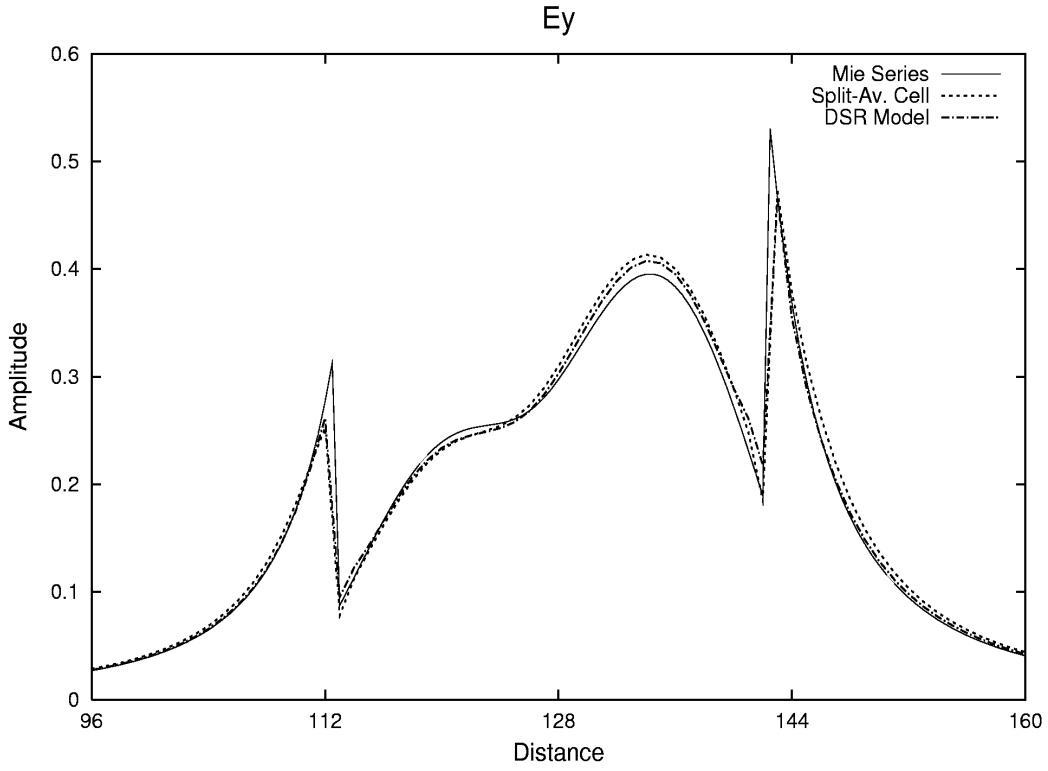


Figure 7a - Magnitude of $E_y$ parallel to y-axis through (x=0,z=1). Compared are DSR and simple averaging. Case II, f=1.767 GHz, and ε=8, 10 points/wavelength. Figure 8b is same as 8a but with 20 points/wavelength.

**Table I**
Amplitudes of Transmitted and Reflected Waves
Second-Order, ε=4.0, 14°, λ/10

| | Split Cell | Standard Cell | Exact |
|---|---|---|---|
| Transmitted Amplitude | .660 (.3%) | .655 (1.06%) | .662 |
| Reflected Amplitude | -.335 (3.7%) | -.344 (6.5%) | -.323 |

**Table II**
Amplitudes of Transmitted and Reflected Waves
Second-Order, ε=8.0, 14°, λ/10

| | Split Cell | Standard Cell | Exact |
|---|---|---|---|
| Transmitted Amplitude | .519 (0.0%) | .513 (1.16%) | .519 |
| Reflected Amplitude | -.477 (1.9%) | -.484 (3.4%) | -.468 |

**Table III**
Amplitudes of Transmitted and Reflected Waves
Fourth-Order, ε=4.0, 14°, λ/7.5

| | Split Cell | Standard Cell | Exact |
|---|---|---|---|
| Transmitted Amplitude | .660 (0.3%) | .643 (2.8%) | .662 |
| Reflected Amplitude | -.325 (.6%) | -.351 (8.7%) | -.323 |

**Table IV**
Amplitudes of Transmitted and Reflected Waves
Fourth-Order, ε=8.0, 14°, λ/7.5

| | Split Cell | Standard Cell | Exact |
|---|---|---|---|
| Transmitted Amplitude | .518 (0.3%) | .502 (3.3%) | .519 |
| Reflected Amplitude | -.468 (0.0%) | -.494 (5.6%) | -.468 |